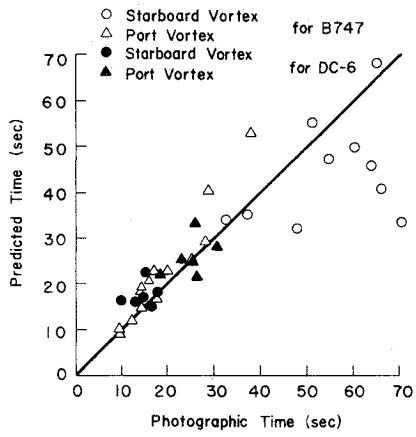

Fig. 3 Comparison of predicted tower hit times vs photographic time for DC-6 and B-747 aircraft flybys.

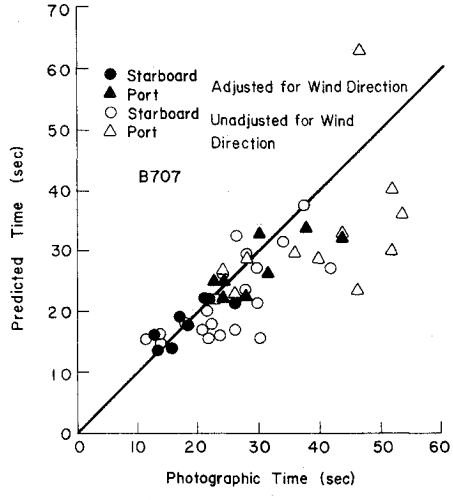

Fig. 4 Comparison of predicted vortex tower-hit times based on power law wind profile vs photographic times.

and a power law profile fit as used in Fig. 1. A power law fit to the mean wind consistently produced better agreement with the vortex tracks partly because of a more accurate wind shear representation at the low altitudes. After about 90 sec the upwind predictive track often lagged behind the data and this is attributed to the rising of the upwind vortex[3] or to a decrease in the circulation of the vortex. The differences between predicted and measured vortex tracks consistently fell within the computed uncertainty in the transport due to random fluctuations in the wind field.

The comparison between predicted and photographically measured times for the vortices to hit the 140-ft tower is shown in Figs. 3 and 4. The wind direction adjustment refers to extrapolation of wind data above the tower to the aircraft cruising altitude (nominally 200 ft).[3] The predicted time is often less than the observed time, especially for older vortices; predicted sink rates based upon elliptical loading assumptions are less than measured rates. There are at least two mechanisms causing the discrepancy, deviations from a clean wing configuration[4] and buoyancy effects[5] leading to decreases in the rolled-up initial vortex separations. Because of the logarithmic variation of the wind magnitude with height, a predicted sink rate which is less than the measured rate will lead to a vortex transport rate in ground effect which is greater than the predicted rate. Uncertainties of up to 25% in the initial vortex separation and 12% in the circulation are contained within the uncertainty in the predicted transport of vortices near the ground due to random fluctuations for winds above 6 fps.

References

[1] Brashears, M. R. and Hallock, J. N., "Aircraft Wake Vortex Transport Model," *Journal of Aircraft*, Vol. 11, May 1974, pp. 265-272.

[2] Hallock, J.N., Wood, W.D., and Spitzer, E.A., "The Motion of Wake Vortices in the Terminal Environment," AMS/AIAA 6th Conference on Aerospace and Aeronautical Meteorology, El Paso, Texas, Nov. 1974.

[3] Brashears, M. R., Hallock, J. N., and Logan, N. A., "Analysis of Predicted Aircraft Wake Vortex Transport and Comparison with Experiment." AIAA Paper 74-506, Palo Alto, Calif., 1974.

[4] Donaldson, C duP., Snedeker, R. S., and Sullivan, R. D., "A Method of Calculating Aircraft Wake Velocity Profiles and Comparison with Full-Scale Experimental Measurements," AIAA Paper 74-39, Washington, D. C., 1974.

[5] Brashears, M. R. and Hallock, J. N., "Buoyancy Effects on the Transport of Aircraft Wake Vortices in Ground Effect," to be published.

Maslen Analysis of Exponential Shocks in a Hypersonic Stream

S. Hariharan* and N. R. Subramanian†
Indian Institute of Technology, Madras, India

Nomenclature

a = bluntness parameter [Eq. (11)]
A = parameter dependent on a [Eq. (11)]
$F(Z)$ = dimensionless body height
h = enthalpy, divided by $U_\infty^2/2$
M = Mach number
p = pressure, divided by $\rho_\infty U_\infty^2$
P = pressure, as in Ref. 1
R_C = shock radius of curvature, Fig. 1
r = lateral dimension, Fig. 1
$S(Z)$ = dimensionless shock height
U = freestream velocity
u,v = velocities in the x,y directions, divided by U_∞, Fig. 1
x,y = shock-oriented coordinates, Fig. 1
Z = streamwise coordinate, nondimensionalized by a characteristic length, Fig. 1
ρ = density, divided by ρ_∞
γ = ratio of specific heats
δ = thickness ratio
ψ = nondimensional stream function
θ = shock wave inclination to oncoming stream

Subscripts

∞ = freestream value
s = behind the shock
o = normal shock
b = body surface

Introduction

CONCAVE shapes are generally encountered on the lower surfaces of two-dimensional wings in hypersonic flight or in the two-dimensional intake of a hypersonic air-breathing engine. Analytical results on the problem of inviscid flow past such shapes are limited in the literature. In a recent paper,[1] Cole and Aroesty have investigated the flow behind concave and convex exponential shock waves within the framework of hypersonic small disturbance theory (HSDT), and have made studies on the optimum shape in the case of concave body.

Received June 3, 1974; revision received August 15, 1974.
Index category: Supersonic and Hypersonic Flow.
*Research Scholar, Department of Aeronautical Engineering.
†Professor and Head, Department of Aeronautical Engineering.

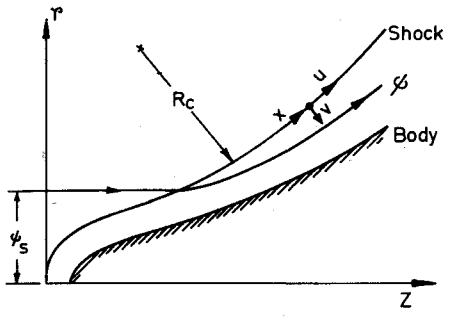

Fig. 1 Shock-oriented coordinate system.

This Note addresses itself to this problem again, and uses the thin shock-layer approximation of Maslen [2] to determine the body shape and pressure distribution behind a slightly blunted exponential shock. For purposes of comparison, the shock shape obtained for flow past exponential two-dimensional shapes [1] have been subjected to the inverse method. [2]

Analysis

Fig. 1 shows a slightly blunted exponential shock, the body that supports this and the shock oriented coordinate system. The equations governing steady hypersonic flow of an adiabatic inviscid gas are written for this system, according to Ref. 2. The variables are nondimensionalized suitably. A von Mises transformation is made, changing to (x,ψ) as the independent variables. On assuming a thin shock layer, ignoring the term $(\partial v/\partial x)_\psi$ as small, and replacing u by its value immediately behind the shock, the transverse momentum equation simplifies to

$$\left(\frac{\partial p}{\partial \psi}\right)_x = \frac{u_s}{R_c} \qquad \text{for the 2-D case} \tag{1}$$

As our region of interest lies not too near the leading edge, the above approximations are fairly valid. On integration, Eq. (1) yields

$$p(x,\psi) = p_s(x) + \frac{u_s(x)}{R_c(x)}\{\psi - \psi_s(x)\} \tag{2}$$

Since in the case of a concave body, the pressure rises from the shock to the body, the above expression for pressure in the layer is modified as

$$p = p_s\{1 + \frac{u_s r_s}{R_c p_s}(1 - \psi/\psi_s)\} \tag{3}$$

This gives the pressure distribution along the body, as $\psi_s = r_s$ and can be expressed as a function of the axial distance. The equation of state is

$$P/\rho^\gamma = f(\psi) \tag{4}$$

The value of p and ρ immediately behind the shock are known from the Rankine-Hugoniot conditions, once the shock geometry is fixed. Combined with Eq. (3), this facilities the determination of ρ in the shock layer. Conservation of energy, after the assumption that $v^2 - v_o^2 << u^2$ gives

$$u = \{2(h_0 - h)\}^{1/2} \tag{5}$$

The above equations, combined with the boundary conditions

$$\psi_s = r_s \text{ and } \psi_b = 0 \tag{6}$$

and the conditions immediately behind the shock, determine the problem of the flowfield completely. Any streamline, and in particular, the body, is obtained by reverting back to the physical plane as

$$r = r_s - u_s \int_{\psi}^{\psi_s} \frac{d\psi}{\rho u} \tag{7}$$

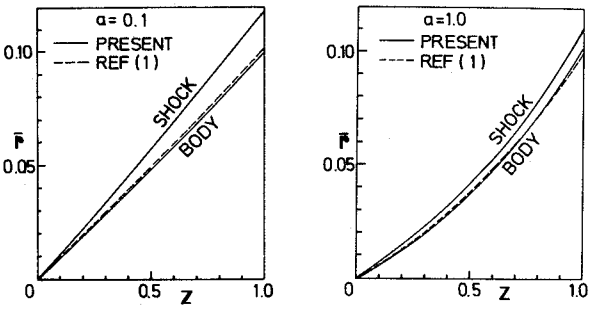

Fig. 2 Body shapes.

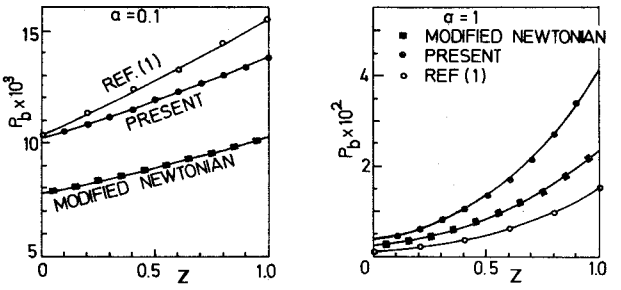

Fig. 3 Pressure distribution along the body surface.

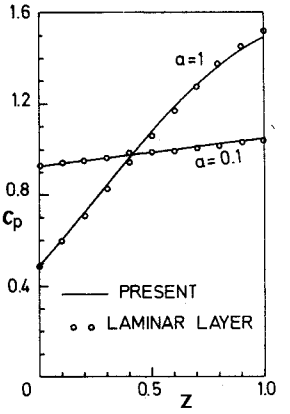

Fig. 4 Comparison of C_p for Maslen and Laminar layer models.

In Ref. 1, a slender aerofoil whose profile is given by†

$$\bar{r} = \delta F(Z), \quad 0 \le Z \le 1, \quad F(0) = 0, \quad F(1) = 1 \tag{8}$$

and the associated shock wave

$$\bar{r}_s = \delta S(Z) \tag{9}$$

in a uniform hypersonic stream corresponding to the limiting case of the hypersonic similarity parameter $1/M_\infty^2\delta^2 \to 0$ is analyzed within the framework of HSDT and assumed attached shock wave. For concave shapes, the pressure distribution is given as

$$p(Z,0) = p_b(Z) = \delta^2[2/(\gamma+1)]A^2P(Z) \tag{10}$$

and the shock shape is

$$S(Z) = (A/a)(e^{aZ} - 1) \tag{11}$$

Positive value for a correspond to shapes concave to oncoming flow. a and A are related by the condition $F(1) = 1$.

These results [1] for two cases (shock shapes) $a = 0.1$ and $a = 1$, have been analyzed by Maslen's method with the object of finding the corresponding body and the pressure distribution. The examples have assumed a thickness ratio δ of 0.1, $\gamma = 1.4$, and $M_\infty = \infty$. Figure 2 shows the resulting body shapes, and Fig. 3 the pressures on the body surface.

Results and Discussion

Body shapes obtained by subjecting the class of shocks obtained as a solution in Ref. 1, to the inverse procedure of Maslen, agree very closely with the body shapes with which [1] it started. However, as anticipated, the pressure distribution along the body surface is different. Though for low shock curvature (lower value of a) the pressures are lower than those given by HSDT, for the higher curvature ($a=1$), the induced pressures are higher than in Ref.1. It would appear that there exists a critical curvature corresponding to some value of a between 0.1 and 1 at which the pressures calculated by the two methods would compare.

For a qualitative comparison, the pressures calculated using the modified Newtonian formula $C_p=C_p^* \sin^2\theta_b$ have also been shown in Fig. 3. For the higher curvature, the pressure so calculated predicts higher values than by the HSDT, as does the present analysis. As a further check, the body surface pressure is obtained using the laminar layer model. [3] Here, an impulse function Q is defined as

$$Q=\int_0 \cos\theta\, d\psi$$

which leads to

$$C_p=2\sin^2\theta+2\sin\theta\cos\theta\frac{d\theta}{dQ} \tag{12}$$

Applying this to an exponential shock, and interpreting the pressure as the sum of the Rankine-Hugoniot pressure immediately behind the shock and a centrifugal correction term, leads to the expression

$$C_p=c_p^*\{\frac{A^2e^{2aZ}}{1+A^2e^{2aZ}}+\frac{A\,e^{aZ}}{(1+A^2e^{2aZ})^{3/2}} \times ln[\frac{A\,e^{aZ}+(1+A^2e^{2aZ})^{1/2}}{A+(1+A^2)^{1/2}}]\} \tag{13}$$

where $C_p^*=4/(\gamma+1)$. This has been plotted in Fig. 4, which also gives the corresponding Maslen pressures. The agreement is excellent.

Conclusions

Exponential shock waves supported by 2-dimensional bodies concave to an oncoming hypersonic stream, for $M_\infty\to\infty$ and $\gamma=1.4$ have been analyzed using the inverse method of Maslen. The body shapes obtained agree well with those given by the HSDT. The Maslen pressures along the surface of the body are higher than those predicted by HSDT, for higher shock curvature. These pressures agree excellently with the pressures calculated using the laminar layer model. A case exists for analyzing in detail the pressures for various nose bluntnesses, as it would help in better drag optimization studies on aerofoils.

References

[1] Cole, J. D. and Aroesty, J., "Hypersonic Similarity Solutions for Aerofoils Supporting Exponential Shock Waves," *AIAA Journal*, Vol. 8, Feb. 1970, pp. 308-315.

[2] Maslen, S. H., "Inviscid Hypersonic Flow Past Smooth Symmetric Bodies," *AIAA Journal*, Vol. 2, June 1964, pp. 1055-1061.

[3] Hayes, W.D. and Probstein, R.F., *Hypersonic Flow Theory*, Vol. 1, 1966, Academic Press, New York, pp. 136-139.

Airframe Noise—The Next Aircraft Noise Barrier

Homer G. Morgan* and Jay C. Hardin†
NASA Langley Research Center, Hampton, Va.

Introduction

PROGRESS in quieting the commercial aviation fleet has been achieved in recent years by reducing the noise generated by turbofan engines on new aircraft. This has been achieved by using higher bypass ratio engines that reduce jet exhaust noise and the application of noise treatment in fan ducts to contain turbomachinery noise. Further technology advancements are expected to make possible additional engine noise reductions. However, further improvements in engine noise reduction mean that nonengine noise sources may become important. References 1 and 2 were among the first in which it was noted that nonpropulsive aerodynamic noise (subsequently referred to as airframe noise) would become the dominant noise source during approach to landing for conventional aircraft designs in which the engines have been quieted to meet more stringent certification requirements. This Note addresses the scope and significance of airframe noise as a new problem in aircraft design by reviewing the present state of the art for its understanding and prediction.

Sources of Airframe Noise

The individual noise sources that combine to produce overall airframe noise of a landing aircraft are illustrated in Fig. 1, and most have been discussed in detail in the literature. [1-4] The main contributors are the turbulent boundary layer; the flow over the extended landing gear, wheel well doors, and wheel well cavities; the flow about the extended flaps and slats; and the wake vorticity associated with lifting surfaces and fuselage. The radiated noise is highly dependent on details of the local flow and, thus, is very configuration dependent.

When a vehicle is aerodynamically "clean," that is, with flaps and gear retracted, the dominant airframe noise is associated with fluctuating lift and drag forces on lifting surfaces. Such unsteady aerodynamic forces can arise from inflow turbulence, from the boundary layer, or from the turbulent wake interacting with the surface. Present estimates are

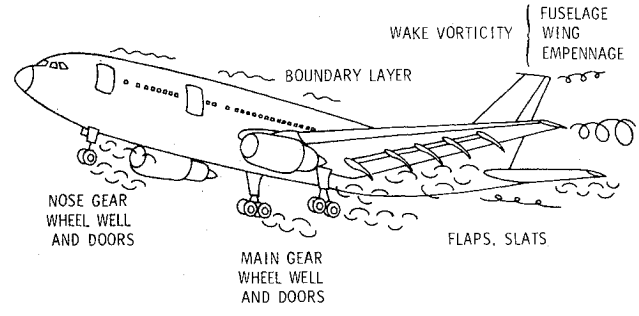

Fig. 1 Airframe noise sources.

Presented as Paper 74-949 at the AIAA 6th Aircraft Design, Flight Test and Operations Meeting, Los Angeles, California, August 12-14, 1974; submitted September 26, 1974; revision received December 26, 1974.

Index category: Aircraft Noise, Aerodynamics (Including Sonic Boom).

*Chief, Acoustics and Noise Reduction Division. Associate Fellow AIAA.

†Head, Surface Interaction Noise Section.